SUBSONIC TO SUPERSONIC NOZZLE FLOWS[*]

O. KRYEZIU[†] AND E. R. JOHNSON[†]

Abstract. Steady, irrotational flow of a compressible fluid through a two-dimensional planar and axisymmetric nozzle is formulated and solved numerically in the hodograph or velocity plane. The Legendre potential is used to express the governing equation which for planar flow is linear and for axisymmetric flow nonlinear. The hodograph transformation method is extended to solve the nozzle problem for supersonic flow. A rectangular numerical domain for the supersonic case results from the way the information travels in the region that is the image of the flow that occurs around the lip of the nozzle surface. Knowledge of the characteristic's exact location in the supercritical region of the domain is not required, but only the general direction in which information propagates.

1. Introduction. The study of air flow through a convergent nozzle is well established and has important practical applications such as in rocketry, the converging propulsive nozzle of a subsonic turbojet engine, and jet engines. This paper discusses two forms of compressible flow: two-dimensional planar and axisymmetric flow. The geometry of the nozzle for planar flow consists of two convergent nozzle walls which extend to upstream infinity, while the axisymmetric nozzle surface is conical. For both cases, the angle δ which the nozzle surface makes with the nozzle center-line is assumed to be within the range $-\pi/2 \leq \delta < 0$. Only the upper half of the physical plane is considered due to symmetry about the center-line.

The hodograph transformation was first applied by Chaplygin [1] to obtain analytical solutions for the nozzle problem in the form of a series of hypergeometric functions. Chaplygin's method is limited to planar subcritical and critical flow, in general. Frankl [2] obtained the value of the discharge coefficient analytically for supersonic choked flow. Norwood [3] solved the two-dimensional supercritical problem numerically in the hodograph plane. He considered the subsonic and supersonic regions separately by modifying iteratively the solution along the sonic line to achieve a continuous solution from one region to the other. The method relies on the linearity of the planar equations in that characteristics are fixed and easily determined in the hodograph plane. Alder [4] developed a numerical method for planar and axisymmetric flow in which the subsonic region is treated in the hodograph plane and the supersonic region in the physical plane by applying the method of characteristics. A matching technique is used to obtain smooth transition of streamlines from one region to the other.

The approach here follows Cook et al. [5], who express the governing equation in terms of the Legendre potential and solve the two-dimensional and axisymmetric nozzle problems for subsonic and sonic flows. Introducing the Legendre potential has

[†]Department of Mathematics, University College London, London, UK (o.kryeziu@gmail.com, e.johnson@ucl.ac.uk).

the advantage that the physical coordinates are given explicitly by the derivatives of the potential. This paper extends the analysis of Cook et al. [5] to supersonic flows by identifying the flow direction angle θ as a time-like variable in the supersonic domain of the hodograph plane. The domain is further extended into a rectangular domain by attaching to it a region in which the Jacobian vanishes. A vanishing Jacobian is associated with nonunique mapping between the hodograph plane and the physical plane [6, 7]. Here, the entire extra region maps into a single point, the corner of the nozzle.

Steady subcritical or critical nozzle flows are characterized by a jet of fluid whose radius smoothly decreases downstream until the density matches the density of the ambient fluid. The supercritical jet differs in that it contracts and expands periodically as it travels downstream from the nozzle. Moving from the subcritical to the supercritical regime, the nature of the governing partial differential equation changes from elliptic to mixed (elliptic and hyperbolic), depending on the region. The jet is calculated here until the flow becomes parallel to the axis. This occurs before any shocks form, and generally close to the nozzle exit.

Section 2 introduces the governing equations and their transformation into the hodograph plane. Section 3 discusses subcritical and critical flows in the physical and velocity planes where the boundary conditions are determined. Section 4 discusses supercritical flow where it is shown that the image in the hodograph domain of the flow field can be taken to be rectangular. The numerical method is developed in section 5, and the results are presented in section 6.

2. Governing equations. All streamlines originate from infinity, where the fluid is taken to be at rest. Downstream, the fluid discharges through the nozzle exit into still fluid. The flow is taken to be homentropic; i.e., the entropy takes the same constant value on each streamline. Under these conditions, the compressible fluid with density ρ, pressure p, and ratio of specific heats γ (for air $\gamma = 1.4$) has speed of sound a defined throughout the flow field as

$$(2.1) \qquad a^2 = \frac{\mathrm{d}p}{\mathrm{d}\rho} \propto \gamma \rho^{\gamma - 1}.$$

In terms of velocity vector components (u, v) parallel to Cartesian coordinates (x, y), the flow is governed by continuity,

$$(2.2) \qquad (a^2 - u^2)u_x - uv(u_y + v_x) + (a^2 - v^2)v_y + k\frac{a^2 v}{y} = 0,$$

irrotationality,

$$(2.3) \qquad u_y - v_x = 0,$$

and Bernoulli's equation,

$$(2.4) \qquad \frac{a^2}{\gamma - 1} + \frac{u^2 + v^2}{2} = \frac{\gamma + 1}{2(\gamma - 1)}a_*^2 = \text{constant},$$

where a_* is the critical speed of sound. For two-dimensional planar flow, $k = 0$; for axisymmetric flow, $k = 1$ and (x, y) are cylindrical coordinates. This is a system of two first order partial differential equations for variables u and v since (2.4) allows the speed of sound to be a function of fluid speed, $V = \sqrt{u^2 + v^2}$.

The two characteristic directions in the (x, y)-plane for (2.2) and (2.3) are

$$(2.5) \qquad C_\pm : \left(\frac{\mathrm{d}y}{\mathrm{d}x}\right)_\pm = \frac{uv \pm a^2\sqrt{M^2 - 1}}{u^2 - a^2},$$

where $M = V/a$ is the Mach number.

2.1. Hodograph transformation. Solving the nozzle problem in the physical (x, y)-plane raises the difficulties of an infinite reservoir and the unknown locations of the jet surface and the sonic line. These can be overcome if instead solutions are sought in the hodograph plane. In this plane, the entire flow field and its boundary conditions can be mapped into a rectangular domain. Regarding x, y as functions of u, v gives the derivatives of u and v as [6]

$$u_x = \frac{y_v}{J}, \quad u_y = -\frac{x_v}{J}, \quad v_x = -\frac{y_u}{J}, \quad v_y = \frac{x_u}{J}$$

for Jacobian $J = x_u y_v - x_v y_u$, which is the reciprocal of the Jacobian in the physical plane j, i.e., $j = u_x v_y - u_y v_x = 1/J$. The Legendre transformation of (2.2)–(2.3) is thus the first order nonlinear system

$$(2.6) \qquad (a^2 - u^2)y_v + uv(x_v + y_u) + (a^2 - v^2)x_u + k\frac{a^2 v}{y}J = 0,$$

$$(2.7) \qquad x_v - y_u = 0.$$

The hodograph transformation is nonsingular so long as J is single-signed. Equation (2.7) implies the existence of the Legendre potential Φ defined by

$$(2.8) \qquad x = \Phi_u, \qquad y = \Phi_v$$

and related to the physical velocity potential ϕ through [6]

$$(2.9) \qquad \Phi = ux + vy - \phi.$$

It is useful to transform the problem into the (M_*, θ)-plane, where $M_* = V/a_*$ is the nondimensional Mach number. Using (2.8) and the relations $u_* = M_* \cos\theta$ and $v_* = M_* \sin\theta$, equation (2.6) becomes [5]

$$
\begin{aligned}
M_*^2 \Phi_{M_* M_*} + f(M_*)(M_* \Phi_{M_*} + \Phi_{\theta\theta}) + k\frac{M_* \sin\theta}{\sin\theta \Phi_{M_*} + \cos\theta \Phi_\theta/M_*}\Big\{ M_* \Phi_{M_*} \Phi_{M_* M_*} \\
+ \Phi_{\theta\theta}\Phi_{M_* M_*} - \left(\Phi_{M_*\theta}^2 - \frac{2\Phi_\theta \Phi_{M_*\theta}}{M_*} + \frac{\Phi_\theta^2}{M_*^2}\right)\Big\} = 0,
\end{aligned}
$$

$$(2.10)$$

where

$$(2.11) \qquad f(M_*) = \frac{(\gamma + 1)(1 - M_*^2)}{(\gamma + 1) - (\gamma - 1)M_*^2}.$$

Variables x and y are related to the derivatives of Φ by

$$(2.12) \qquad x = \Phi_{u_*} = \cos\theta \Phi_{M_*} - \frac{\sin\theta}{M_*}\Phi_\theta,$$

$$(2.13) \qquad y = \Phi_{v_*} = \sin\theta \Phi_{M_*} + \frac{\cos\theta}{M_*}\Phi_\theta.$$

The equations relating density and pressure to their stagnation values ρ_0, p_0 for an isentropic process are

$$(2.14\text{a,b}) \qquad \frac{\rho}{\rho_0} = \left(1 - \frac{\gamma-1}{\gamma+1}M_*^2\right)^{1/(\gamma-1)}, \qquad \frac{p}{p_0} = \left(1 - \frac{\gamma-1}{\gamma+1}M_*^2\right)^{\gamma/(\gamma-1)}.$$

Along the free-streamline, (2.14b) relates the pressure ratio to the free-streamline speed.

For planar flow, $k = 0$, the characteristics of (2.10) are given as integrals of two ordinary differential equations,

$$(2.15) \qquad \Gamma_\pm : \left(\frac{\mathrm{d}\theta}{\mathrm{d}M_*}\right)_\pm = \pm\frac{\sqrt{-f(M_*)}}{M_*}.$$

Therefore, their location in the supersonic region of the hodograph domain is fixed and independent of the solution $\Phi(M_*, \theta)$. Clearly, where $M_* < 1$ the Γ-characteristics are imaginary, and where $M_* > 1$ two families of characteristics exist. Under the hodograph transformation, $\Gamma_\pm$ are images of Mach waves of the physical plane characteristics $C_\pm$, respectively [6, 8]. For axisymmetric flow, Γ-characteristics are no longer predetermined in the hodograph plane since they depend on the solution Φ.

3. Subsonic and sonic flow. The flow is subsonic if $M_* < 1$ on the free-streamline and sonic if $M_* = 1$. The governing equations are elliptic and solutions smooth and infinitely differentiable. Substituting $M_* = 1$ into (2.14b) yields the critical pressure ratio.

A sketch of the sonic jet, corresponding to both two-dimensional and axisymmetric flow, is shown in Figure 3.1. The flow originates from a stagnation state far upstream of an infinite reservoir, OO. The nozzle surface BO extends to infinity at a constant angle δ to the center-line and is given in the (x, y)-plane by $y = H + (x - x_0)\tan\delta$, where H is the size of the half-orifice, x_0 is a value of x where the origin is set, and $x \leq x_0$.
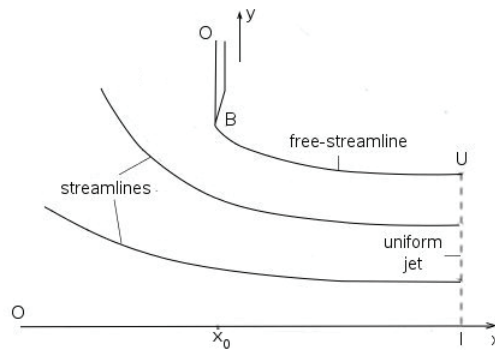
FIG. 3.1. *The sonic jet in the physical plane for $\delta = -\pi/2$. Streamlines originating from far upstream become parallel to the center-line at a finite distance from the exit plane.*

As the fluid discharges downstream it forms a jet bounded by the free-streamline BU and the x-axis. Far downstream all streamlines of the jet eventually become parallel and the jet radius remains constant. The speed along BU is constant and is determined from the pressure ratio. If this speed is subsonic, a uniform subsonic

state across the jet is reached at an infinite distance from the nozzle. Ovsiannikov [9] shows that if the speed is sonic, the jet achieves a uniform state at a finite distance from the nozzle's exit.

Mapping the physical domain into the (M_*, θ)-plane gives the rectangular domain shown in Figure 3.2. The image of the uniform downstream jet in the hodograph plane is represented by point U, I. At this isolated point J is infinite, corresponding to multiple solutions of x and y.
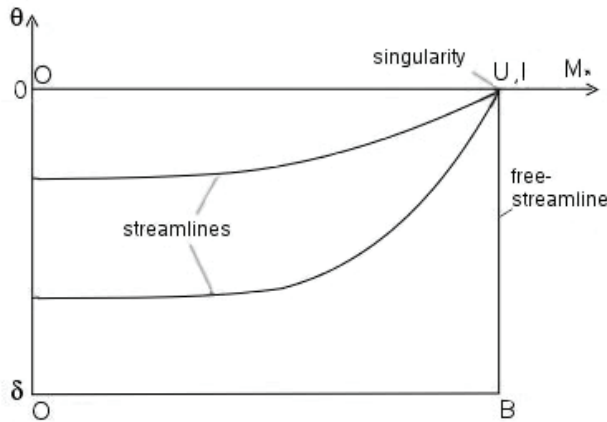
FIG. 3.2. *The hodograph representation of sonic or subsonic flow. On OO $\Phi = constant$, on OB $\Phi_\theta = M_*(H\cos\delta - x_0\sin\delta)$, on OU $\Phi_\theta = 0$, on BU $M_{*B}\Phi_{M_*} + \Phi_{\theta\theta} = 0$, and at B $\Phi_\theta = M_{*B}(H\cos\delta - x_0\sin\delta)$, $\Phi_{M_*} = x_0\cos\delta + H\sin\delta$.*

3.1. Boundary conditions. Far upstream density variations are small and the flow is essentially incompressible sink-flow. For the planar problem, the upstream condition is

$$(3.1) \qquad \phi = -m\log r \qquad \text{as} \qquad r \to \infty,$$

where $r = (x^2 + y^2)^{1/2}$ and m, a constant, is the strength of the sink. Substituting

$$(3.2) \qquad u_* = \phi_x = -\frac{mx}{r^2} \quad \text{and} \quad v_* = \phi_y = -\frac{my}{r^2}$$

into (2.9) and using $r^2 = m^2/M_*^2$ gives

$$(3.3) \qquad \Phi = -m + m\log\frac{m}{M_*} \quad \text{on} \quad OO.$$

This Dirichlet boundary condition is singular when $M_* = 0$; however, the condition is also valid when M_* is sufficiently small. Denoting $M_{*O} > 0$ to be as such, the domain can be truncated on the left to begin at M_{*O}. Likewise, for the axisymmetric case, the far upstream condition for the velocity potential is

$$(3.4) \qquad \phi \propto r^{-1} \qquad \text{as} \qquad r \to \infty,$$

which in terms of the Legendre potential and M_* becomes

$$(3.5) \qquad \Phi \propto \sqrt{M_*} \quad \text{on} \quad OO.$$

Thus, for both planar and axisymmetric flow, the Dirichlet boundary condition $\Phi =$ constant can be applied on OO.

Along the x-axis, i.e., on $y = 0$, flow direction is $\theta = 0$, so

$$(3.6) \qquad \Phi_\theta = 0 \quad \text{on} \quad OI.$$

Here the line OI along the x-axis is equivalent to OU in the hodograph plane since there I and U map into the same point, as shown in Figure 3.2.

Since the nozzle wall makes an angle δ with the horizontal, this is also the flow direction angle of the bounding streamline, i.e., $\theta = \delta$. Substituting (2.12), (2.13) into the wall equation $y = H + (x - x_0)\tan\delta$ gives the boundary condition

$$(3.7) \qquad \Phi_\theta = M_*(H\cos\delta - x_0\sin\delta) \quad \text{on} \quad OB.$$

On the free-streamline $\mathrm{d}y/\mathrm{d}x = v/u$ and using the expressions $\mathrm{d}x = x_u\mathrm{d}u + x_v\mathrm{d}v$ and $\mathrm{d}y = y_u\mathrm{d}u + y_v\mathrm{d}v$ yields

$$(3.8) \qquad u(y_u\mathrm{d}u + y_v\mathrm{d}v) = v(x_u\mathrm{d}u + x_v\mathrm{d}v).$$

Substituting $u\mathrm{d}u + v\mathrm{d}v = 0$ into (3.8) to eliminate $\mathrm{d}u$ and $\mathrm{d}v$, the PDE valid along the free-streamline is given by Cook et al. [5]:

$$(3.9) \qquad v^2 x_u - uv(y_u + x_v) + u^2 y_v = 0.$$

Expressing this in terms of the Legendre potential and M_* gives

$$(3.10) \qquad \Phi_{\theta\theta} + M_{*B}\Phi_{M_*} = 0 \quad \text{on} \quad BU.$$

This completes the specification of Φ on the boundaries of the flow region. It is necessary to supply another boundary condition to specify the scale of the problem. Let the width of the jet when it becomes uniform far downstream, i.e., when $\theta = 0$, be denoted by w. Then (2.13) gives [5]

$$(3.11) \qquad \Phi_\theta = M_{*B}w \quad \text{at point} \quad U, I.$$

It is also possible to instead impose the size of the nozzle's exit H as the desired scale and x-coordinate x_0 by applying at point B the two boundary conditions

$$(3.12) \qquad \Phi_{M_*} = x_0\cos\delta + H\sin\delta,$$

$$(3.13) \qquad \Phi_\theta = M_{*B}(H\cos\delta - x_0\sin\delta),$$

which can be derived using (2.12) and (2.13).

4. Supersonic flow. When the pressure ratio is below the critical value, the outer surface of the jet has speed $M_* > 1$ and the flow is supersonic. Equations (2.2), (2.3) are of mixed type, elliptic in the subsonic domain ($M_* < 1$) and hyperbolic in the supersonic domain ($M_* > 1$). On the sonic line the system is parabolic.

Figure 4.1 shows a supersonic jet in the physical plane based on a figure from Guderley [7]. As in the preceding section, the flow originates from far upstream and is bounded by the nozzle surface OB, the free-streamline BF, and the x-axis. The supersonic jet differs from the subsonic and sonic jets in that, a short distance from the exit plane, it contracts to a minimum area to form a vena contracta [4]. Ignoring frictional interaction with the ambient fluid, further downstream the fluid

FIG. 4.1. *Supersonic flow in the physical plane for $\delta = -\pi/2$. The curves (dashed lines) emanating from corner B are rarefaction waves. They are reflected from the sonic line BC as compression waves, which are shown by solid lines. The problem is solved in the hodograph plane up to UC where $\theta = 0$.*

expands and contracts periodically [10]. Around the sharp corner B, the flow expands isentropically as a Prandtl–Meyer expansion fan consisting of an infinite number of Mach waves emanating from the corner B [7]. The Mach waves approaching the sonic line are rarefaction waves and are reflected from the sonic line as compression waves. Rarefaction waves are shown by dashed lines in Figure 4.1 and compression waves by solid lines. Any boundary condition prescribed at a point on the free-streamline will exert an influence on the subsonic region, provided a characteristic runs from that point to the sonic line. The last of such characteristics to propagate information to the sonic line from the jet surface is shown in Figure 4.1 as the rarefaction wave EC. Hence, region DEC represents that part of the supersonic region whose solution can only be obtained by simultaneous calculation with the subsonic region of the flow field.

The flow in the physical plane shown in Figure 4.1 when mapped into the hodograph (M_*, θ)-plane results in the domain shown in Figure 4.2. As for sonic flow, the subsonic region maps into a rectangular domain, $OBCO$. The supersonic region $BDFC$, which meets the subsonic region along the sonic line BC, is covered by an infinite number of characteristics belonging to the two characteristic families $\Gamma_\pm$.

The boundary conditions far upstream at OO, on the x-axis OC, along the wall OB, and on the free-streamline DF are unchanged from the respective conditions for subsonic and sonic jets. At B in the physical plane the bounding streamline OBF turns abruptly while its velocity increases to the free-streamline value. Hence B, which is a single point in the physical plane, is represented by the entire line BD in the hodograph plane (see Figure 4.2). On the curve BD

$$(4.1\mathrm{a,b}) \qquad \mathrm{d}x = x_{M_*}\mathrm{d}M_* + x_\theta\mathrm{d}\theta = 0, \qquad \mathrm{d}y = y_{M_*}\mathrm{d}M_* + y_\theta\mathrm{d}\theta = 0,$$

from which

$$(4.2) \qquad\qquad J = x_{M_*}y_\theta - x_\theta y_{M_*} = 0.$$

FIG. 4.2. *Supersonic flow in the hodograph plane. Two families of Γ-characteristics cover the supersonic region BDFC. Dashed lines are image to rarefaction waves, and solid lines to compression waves.*

Using (4.1a) and (2.12) the slope of curve BD can be written in the form

$$(4.3) \qquad \frac{\mathrm{d}\theta}{\mathrm{d}M_*} = -\frac{x_{M_*}}{x_\theta} = -\frac{\left(\Phi_{M_* M_*}\cos\theta + \frac{1}{M_*^2}\Phi_\theta\sin\theta - \frac{1}{M_*}\Phi_{M_*\theta}\sin\theta\right)}{\left(\Phi_{M_*\theta}\cos\theta - \Phi_{M_*}\sin\theta - \frac{1}{M_*}\Phi_{\theta\theta}\sin\theta - \frac{1}{M_*}\Phi_\theta\cos\theta\right)}.$$

Combining (2.10), the Jacobian equation is expressed as

$$(4.4) \qquad J = -\left[\left(\frac{1}{M_*}\Phi_{M_*\theta} - \frac{1}{M_*^2}\Phi_\theta\right)^2 + f(M_*)\left(\frac{1}{M_*}\Phi_{M_*} + \frac{1}{M_*^2}\Phi_{\theta\theta}\right)^2\right] = 0,$$

and (4.3) gives

$$(4.5) \qquad \frac{\mathrm{d}\theta}{\mathrm{d}M_*} = \pm\frac{\sqrt{-f(M_*)}}{M_*}.$$

This shows that the curve BD, besides being a streamline, is also a Γ-characteristic for both planar and axisymmetric flow. Guderley [7, p. 85] shows that if the Jacobian expressed in terms of the streamfunction vanishes along a streamline but both its terms do not, then the streamline and the characteristic coincide. A consequence of BD being a characteristic is that while Φ, Φ_{M_*}, Φ_θ are uniquely determined, derivatives of second order may be discontinuous on BD.

The curve BD may be regarded as an initial curve and the two boundary conditions (3.12), (3.13) prescribed on it as initial conditions. Therefore, θ can now be perceived as the time-like variable in the supersonic domain $BDFC$ as two boundary conditions are prescribed on characteristic BD and no boundary condition on CU (see Figure 4.2). Integrating (3.12) and (3.13) gives the value of Φ on BD as

$$(4.6) \qquad \Phi(M_*,\theta) = M_*(H\sin\theta + x_0\cos\theta) + \text{constant}.$$

This is a solution of the governing equation (2.10) for both planar and axisymmetric flow, and it satisfies identically the condition on the free-streamline, (3.10). Hence, the supersonic domain can be extended by attaching to it region BAD, as shown in Figure 4.3, without affecting the solution of the entire problem. Consider BA as the initial line and apply there (3.12) and (3.13), while along AD impose (3.10). These conditions together with the governing equation (2.10) constitute an initial boundary value problem on region BAD whose solution is (4.6), which also holds on BD. Therefore, the values $x = x_0$ and $y = H$ will propagate unchanged, from line BA up to characteristic BD, which implies that the image of region BAD in the xy-plane is a single point, the corner B. Along BD, two distinct integral surfaces touch: one given by (4.6) and the other determined by the solution of the problem.

The advantage of introducing region BAD is that finite difference methods can be applied in a rectangular mesh, avoiding the need to impose the boundary conditions (3.12) and (3.13) on the characteristic curve BD in the hodograph plane.

FIG. 4.3. *The extended hodograph plane for supercritical flow. Region BAD has been attached to the characteristic BD. Region CFU is covered more than once by the streamlines. Along the edge CF the Jacobian J is infinite.*

The flow is choked if the mass flow rate discharging from the nozzle reaches its maximum limit. Then point E in Figure 4.1 moves to point D, and all the rarefaction waves that meet the sonic line emanate from the edge, as shown in Figure 4.4. Considering Figure 4.5, to obtain choked flow the supersonic domain of the hodograph plane has to be extended in the increasing M_* direction up to or beyond the point where two characteristics BD and CE intersect. Since the position of the characteristics for two-dimensional planar flow is known, it is possible to determine the choking free-streamline velocity denoted here as M_{*c}. Letting $b = (\gamma + 1)/(\gamma - 1)$, for planar flow $k = 0$, (2.15) can be integrated to yield the equation of BD as

$$(4.7) \qquad \theta = \sqrt{b}\tan^{-1}\left(\frac{M_*^2 - 1}{b - M_*^2}\right)^{1/2} - \tan^{-1}\left(\frac{M_*^2 - 1}{1 - M_*^2/b}\right)^{1/2} + \delta.$$

FIG. 4.4. *Sketch of choked flow based on a figure from Guderley [7]. No rarefaction waves from the jet-surface intersect point C or the sonic line BC.*

FIG. 4.5. *The hodograph domain when the flow is choked. The point of intersection of characteristics BD and CE gives the least value of free-streamline velocity M_{*c} which yields choked flow.*

The equation of characteristic CE is

$$(4.8) \qquad \theta = -\sqrt{b}\tan^{-1}\left(\frac{M_*^2 - 1}{b - M_*^2}\right)^{1/2} + \tan^{-1}\left(\frac{M_*^2 - 1}{1 - M_*^2/b}\right)^{1/2}.$$

Eliminating θ from these two equations, the value M_{*c} at the point of intersection satisfies

$$(4.9) \qquad \sqrt{b}\tan^{-1}\left(\frac{M_{*c}^2 - 1}{b - M_{*c}^2}\right)^{1/2} - \tan^{-1}\left(\frac{M_{*c}^2 - 1}{1 - M_{*c}^2/b}\right)^{1/2} + \delta/2 = 0.$$

For the two-dimensional case ($\delta = -\pi/2$), $M_{*c} = 1.9045$ is the smallest value of M_* that can be prescribed on the free-streamline for flow to choke. In the axisymmetric

case, the location of CE is not known initially; hence the choking pressure ratio is obtained once the solution is computed numerically.

Reducing the downstream pressure further to the zero limit yields the maximum value $M_* = 2.4495$ attained by the fluid for the nozzle problem, i.e., the velocity at which gas expands into a vacuum.

5. Numerical integration. The rectangular hodograph planes shown in Figure 3.2 for the subcritical problem and region $OAUO$ in Figure 4.3 for the supercritical problem promote the use of finite difference methods to numerically integrate the governing equation and the boundary conditions. The computational domain is subdivided into a uniform grid with n_c columns and n_r rows so that the coordinates M_* and θ at any mesh node (i, j) of the grid are given by a discrete representation,

$$M_{*i} = M_{*O} + (i-1)\Delta M_*, \quad i = 1, 2, \ldots, n_c,$$
$$\theta_j = -(j-1)\Delta\theta, \quad j = 1, 2, \ldots, n_r,$$

where ΔM_* and $\Delta\theta$ are constant grid spacings of the M_*- and θ-coordinates. The values M_{*1} and M_{*n_c} correspond to the upstream and downstream M_*-boundaries, respectively. The type of problem solved depends on the value given to M_{*n_c}. Choose $M_{*n_c} < 1$ for subsonic flow, $M_{*n_c} = 1$ for sonic flow, and $M_{*n_c} > 1$ for supersonic flow. Similarly, $\theta_1 = 0$ and $-\pi/2 \le \theta_{n_r} < 0$ are the bounding values of the θ-coordinate, where θ_{n_r} is the angle the nozzle wall makes with the horizontal, i.e., $\theta_{n_r} = \delta$. The value of the function $\Phi(M_*, \theta)$ at mesh node (i, j) is specified as

$$(5.1) \qquad \Phi(M_{*i}, \theta_j) = \Phi_{i,j} \qquad i, j = 1, 2, \ldots.$$

Results vary little for $0 < M_{*O} < 1$, and so in the computations below M_{*O} is set at 0.04. Then the value of Φ along M_{*O} can be chosen arbitrarily. All the boundary conditions in the domain are Neumann except far upstream, along OO, where a Dirichlet boundary condition is applied. The solution in the physical plane is unique, but the surface Φ is determined only to within an additive constant in the hodograph plane.

For subcritical and critical flow, (2.10) and the boundary conditions constitute an elliptic boundary value problem. Centered differences are used in the domain except on the free-streamline boundary where one sided differences are used. Two ghost cells are introduced to preserve second order accuracy on the boundaries corresponding to the wall and axis of symmetry. For supercritical flow, (2.10) has different type in different regions; consequently, each region requires its own consideration when applying the numerical method. In the subsonic region of the domain centered differences are applied, but in the supersonic region numerical integration must be performed in accordance with the time-like propagation of information. Backward differences are used at each mesh node in the supersonic domain. The PDE is estimated at level j and the derivatives Φ_θ, $\Phi_{\theta\theta}$, $\Phi_{M_*\theta}$ are replaced by backward difference approximations,

$$\Phi_\theta \mid_{ij} \approx \frac{3\Phi_{i,j} - 4\Phi_{i,j+1} + \Phi_{i,j+2}}{2\Delta\theta},$$
$$\Phi_{\theta\theta} \mid_{ij} \approx \frac{\Phi_{i,j} - 2\Phi_{i,j+1} + \Phi_{i,j+2}}{\Delta\theta^2},$$
$$\Phi_{M_*\theta} \mid_{ij} \approx \frac{3\Phi_{i+1,j} - 4\Phi_{i+1,j+1} + \Phi_{i+1,j+2}}{4\Delta\theta\Delta M_*} - \frac{(3\Phi_{i-1,j} - 4\Phi_{i-1,j+1} + \Phi_{i-1,j+2})}{4\Delta\theta\Delta M_*}.$$

The M_* derivatives are also estimated at node (i, j). The first and the third approximations are second order accurate, whereas the second is only first order accurate. The von Neumann stability analysis for the linear planar flow equation shows that the scheme is unconditionally stable.

5.1. Solution of the algebraic system of equations. Due to linearity, the algebraic system of equations is constructed and solved first for the two-dimensional planar problem. Substituting the described approximations into (2.10) ($k = 0$) and into the appropriate boundary conditions leads to a linear system of equations. This system can be written as the matrix equation

$$(5.2) \qquad\qquad\qquad A \cdot \boldsymbol{\Phi} = \mathbf{b},$$

where A is the coefficient matrix, $\boldsymbol{\Phi}$ is the vector of the unknown values Φ_k at each mesh node, $k = 1, 2, \ldots, n_r n_c + 2n_c$, and $\mathbf{b}$ is the vector of the right-hand sides. The coefficient matrix A is sparse, meaning that few elements are nonzero relative to the number of zero elements.

For the axisymmetric problem, the resulting system consists of a set of nonlinear algebraic equations. Solutions are obtained using an iterative process by generating a sequence of successive approximations for $\boldsymbol{\Phi}$ and A where the planar flow solution, denoted as $\boldsymbol{\Phi}^0$, is used as an initial guess to start the iterations. The iterative sequence is described by the recurrence formula

$$(5.3) \qquad\qquad\qquad A^n \boldsymbol{\Phi}^{n+1} = \mathbf{b}, \qquad n = 0, 1, \ldots,$$

where n is the iteration number. After each iteration, the computed values of vector $\boldsymbol{\Phi}$ are used to update the entries of matrix A so that the system can be resolved for $\boldsymbol{\Phi}$. It is advantageous to introduce a relaxation factor ω to speed up the rate of convergence and to maintain stability of the iterative process. In vector form the process is described as

$$(5.4) \qquad\qquad\qquad A[\boldsymbol{\Phi}^0]\boldsymbol{\Phi}^1 = \mathbf{b},$$

$$(5.5) \qquad A[\boldsymbol{\Phi}^{n-1} + \omega(\boldsymbol{\Phi}^n - \boldsymbol{\Phi}^{n-1})]\boldsymbol{\Phi}^{n+1} = \mathbf{b}, \qquad n = 1, 2, \ldots.$$

6. Numerical results. Once the hodograph solution $\Phi(M_*, \theta)$ is obtained, the physical coordinates are retrieved by applying (2.12) and (2.13) along lines of constant M_*. Isolines of normalized density and pressure computed using relations (2.14) for critical planar and axisymmetric flow are plotted in Figures 6.1(a) and 6.1(b). The x-coordinate displayed states the distance away from the nozzle's exit plane at which the jet becomes uniform. For axisymmetric flow this distance is shorter but the width of the jet is greater. The isolines depict the adjustment in pressure which the flow undergoes from upstream infinity where pressure is high to the downstream fluid where the pressure is low. Figures 6.2(a) and 6.2(b) show isolines of normalized density and pressure of supercritical choked flow with free-streamline velocity $M_* = 2$ for both planar and axisymmetric flow. The axisymmetric jet surface has the vena contracta at a shorter distance from the nozzle's exit plane.
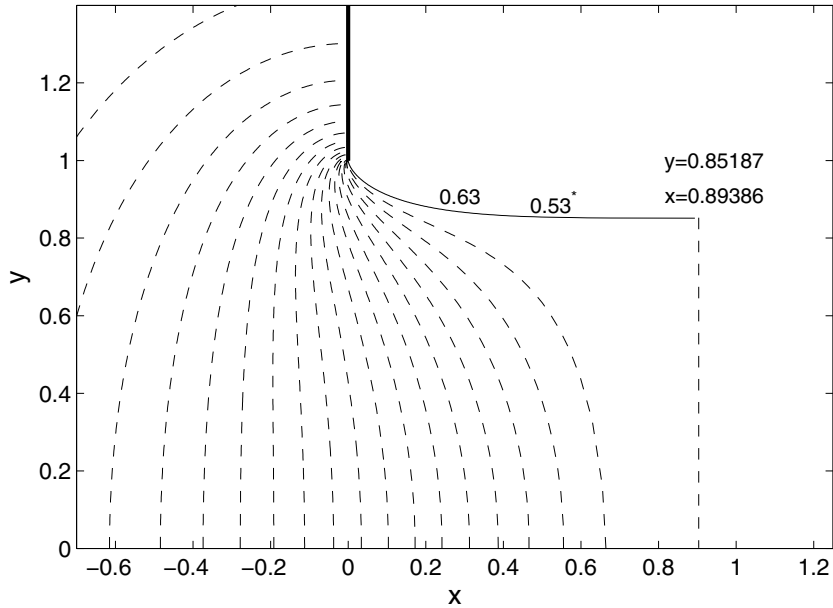
The discharge coefficient, denoted as C_d, is defined as

$$(6.1) \qquad\qquad\qquad C_d = \frac{\dot{m}}{\dot{m}_{1D}},$$

where $\dot{m}$ is the actual rate of mass flow and $\dot{m}_{1D}$ is the one-dimensional ideal mass flow rate. The actual mass flow rate $\dot{m}$ is calculated by integrating the solution along
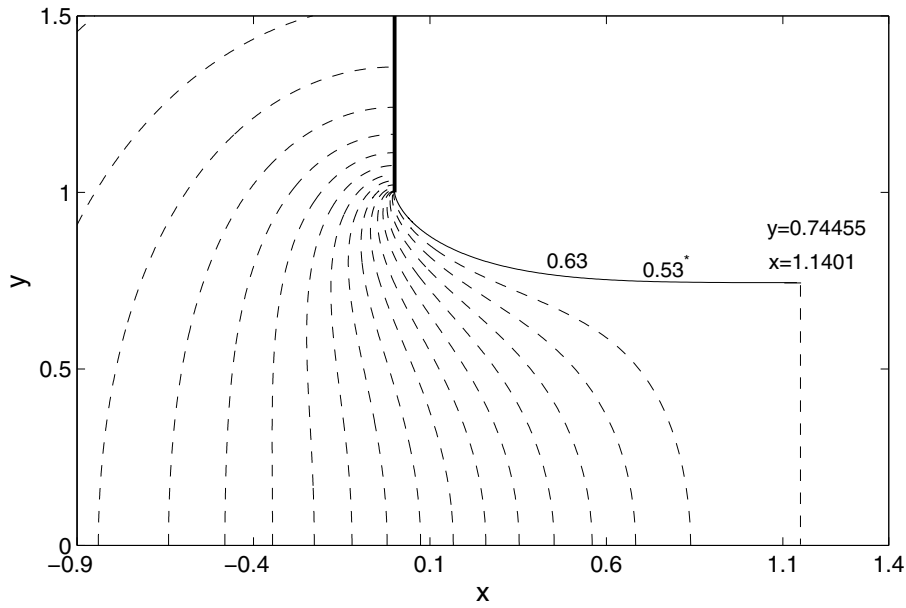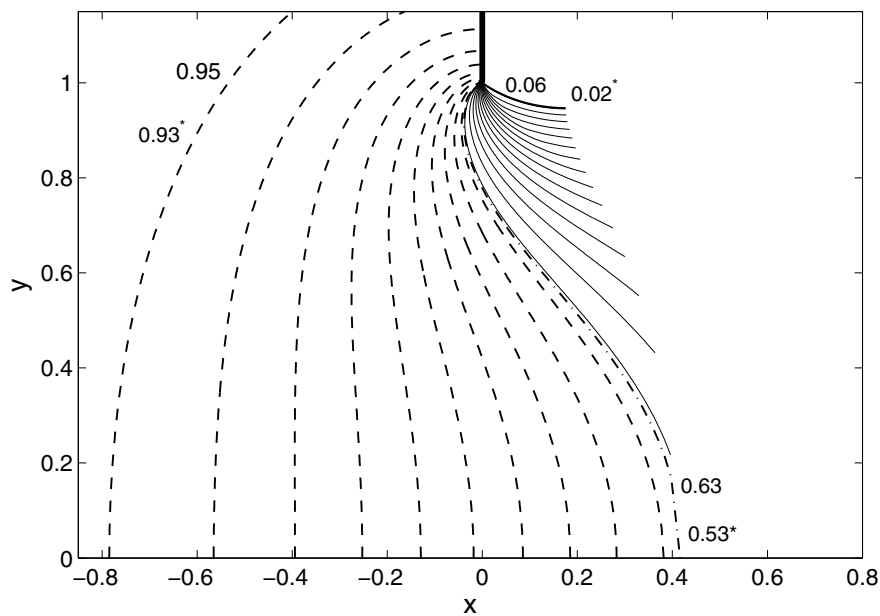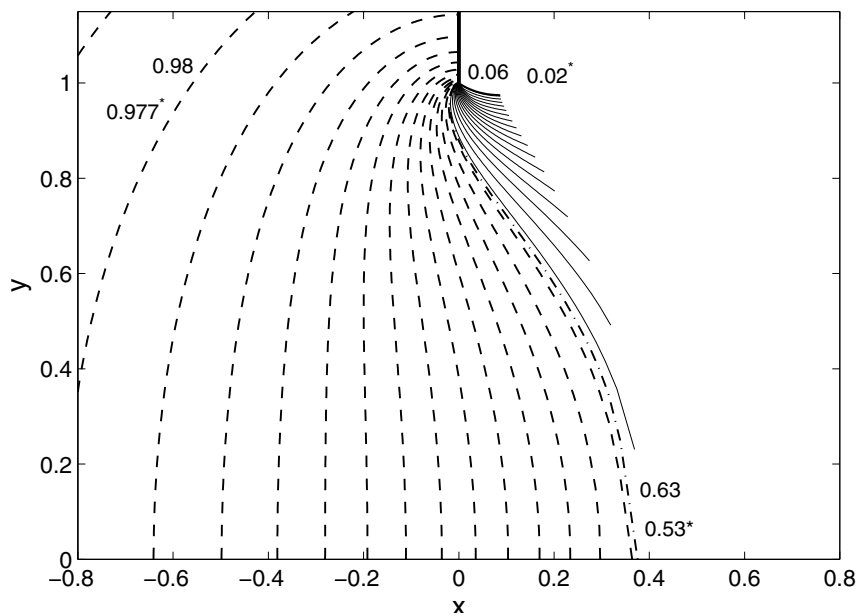
(a) Planar

(b) Axisymmetric

FIG. 6.1. *Sonic jets. The values labeled on the isolines state the normalized density ρ/ρ_0. Those with superscript $(*)$ denote the normalized pressure p/p_0.*

(a) Planar

(b) Axisymmetric

FIG. 6.2. *Supersonic choked jets, $M_* = 2$ on the free-streamline. The values labeled on the isolines state the normalized density ρ/ρ_0. Those with superscript $(*)$ denote the normalized pressure p/p_0. Dashed lines indicate that isolines lie in the subsonic region, and the solid lines indicate that they lie in the supersonic region. The vena contracta is closer to the exit plane for axisymmetric flow.*

lines of constant M_* in the (x, y)-plane and is given as

$$(6.2) \qquad \dot{m} = \int_c \rho \mathbf{u} \cdot \vec{\mathbf{n}} (2\pi y)^k dl,$$

where $\mathbf{u}$ is the velocity vector and $\vec{\mathbf{n}}$ is a unit vector perpendicular to the curve c of constant M_*. Simpson's rule is chosen as the method of numerical integration. Since the flow is considered to be steady, $\dot{m}$ is constant along each constant M_* line of the subsonic region. The ideal mass flow rate $\dot{m}_{1D}$ assumes one-dimensional uniform flow parallel to the x-axis. At corner B, the mass flux is calculated using

$$(6.3) \qquad \dot{m}_{1D} = (\pi y_B)^k M_{*B} \rho_B y_B.$$

For the two-dimensional case $(k = 0)$ (6.2) and (6.3) give the discharge coefficients by integration across half the nozzle, whereas for axisymmetric flow $(k = 1)$ the integration is across the whole nozzle. Figures 6.3(a) and 6.3(b) show plots of computed C_d against free-streamline speed M_* for planar and axisymmetric flow at various nozzle wall angles δ. As is anticipated, in both cases, the discharge coefficient increases with an increase in free-streamline speed. A higher rate of discharge is achieved as the magnitude of the wall angle $|\delta|$ is reduced with the limit being that of straight channel flow, i.e., $C_d = 1$ as $|\delta| \to 0$.

Table 6.1(a) shows values of C_d for planar and axisymmetric sonic jet, $M_* = 1$, as a function of mesh size. Starting with a relatively coarse grid, $(n_c, n_r) = (49, 201)$, the spacings are halved and C_d recalculated. In both flow cases considered, the discharge coefficient systematically converges to the final value obtained on the fine grid. For the two-dimensional jet the difference in C_d obtained from the coarse and finest grids is less than $3 \cdot 10^{-4}$, and for the axisymmetric jet it is 0.001. The sonic discharge coefficients match those of Alder [4] to at least 3 decimal places and are in close agreement with those of Cook et al. [5]. As the jet speed is gradually increased to its choking value M_{*c}, the discharge coefficient also approaches its choking value. These limiting values of C_d are displayed in Table 6.1(b) for both two-dimensional and axisymmetric flow. The difference in C_d, for the two-dimensional jet, between the initial and final grids, is $7.8 \cdot 10^{-4}$, and for the axisymmetric jet it is 0.001. A higher discharge rate is achieved in two-dimensional flow compared with axisymmetric flow, consistent with Alder [4].

Figure 6.4 shows the location of free-streamlines computed as the initial grid is refined for two-dimensional supersonic choked flow with $M_* = 2$. The change in location is systematic and very small: the lower line comes from the coarse grid and the upper one from the fine grid.

Further notes on the numerical technique:

• A stopping criterion for (5.5) is established by substituting the computed solution into the discretized form of the governing equation so that the residue in each mesh node can be used as a measure of the error. The number of iterations depends on the relaxation factor ω. If $\omega = 0.4$, 70 iterations reduce the residue to less than 10^{-8}. Fewer iterations are needed if ω is greater.

• It appears from numerical experiments that for axisymmetric supersonic flow, $M_* \gtrsim 1.8$, the stability of the numerical process becomes dependent on the ratio of grid spacings $\Delta\theta / \Delta M_*$ even when backward differences are used. Due to this, the initial grid is halved up to three times for the choked flow in Table 6.1(b). No difficulties are encountered for the two-dimensional supersonic jet.

• Characteristic BD for axisymmetric flow is the same as for two-dimensional flow, and hence its location is known. Characteristic CE is unknown in this case due
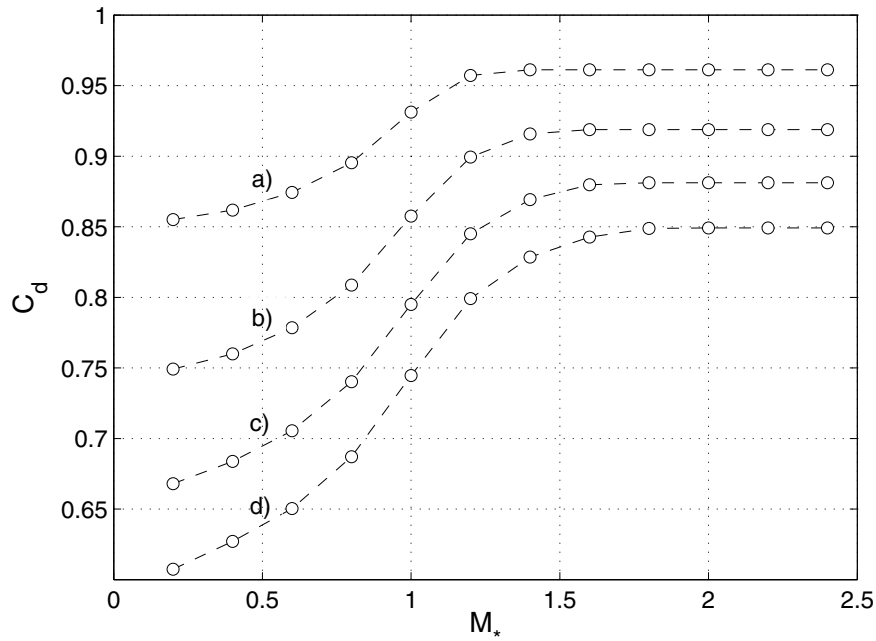
(a) Planar
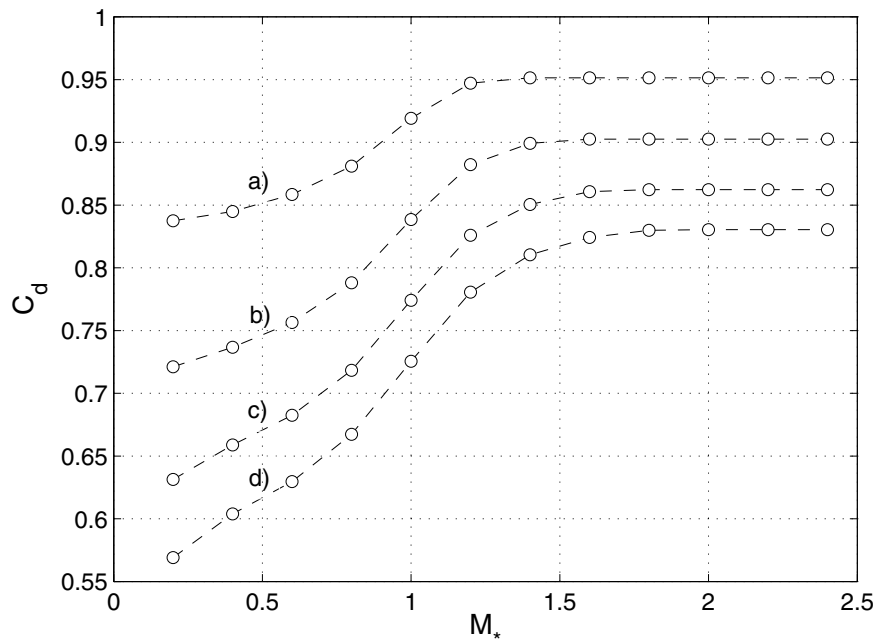
(b) Axisymmetric

Fig. 6.3. *Discharge coefficient at various nozzle wall angles. Flow solved from subcritical to supercritical choked flow.* a: $\delta = -\pi/8$. b: $\delta = -\pi/4$. c: $\delta = -3\pi/8$. d: $\delta = -\pi/2$.

TABLE 6.1

The discharge coefficient, for $-\delta = \pi/2$, as a function of mesh size. The initial coarse mesh has $(\Delta M_*, \Delta\theta) = (\Delta M_{*i}, \Delta\theta_i) = (0.02, 0.0079)$. Subsequent meshes have $(\Delta M_*, \Delta\theta) = 2^{-N}(\Delta M_{*i}, \Delta\theta_i)$ for $N = 1, 2, \ldots$.

(a) Sonic flow

$2^{-N}(\Delta M_{*i}, \Delta\theta_i)$	Two-dimensional	Axisymmetric
$N = 0$	0.74428	0.7247
1	0.74448	0.7254
2	0.74453	0.7256
3	0.74454	0.7257
4	0.74455	0.7257
Cook et al. [5]	0.7455	0.7292
Alder [4]	0.7445	0.726

(b) Choked flow, $M_* = 2$

$2^{-N}(\Delta M_{*i}, \Delta\theta_i)$	Two-dimensional	Axisymmetric
$N = 0$	0.85011	0.83143
1	0.84965	0.83081
2	0.84943	0.83054
3	0.84933	0.83043
Alder [4]	0.849	0.830
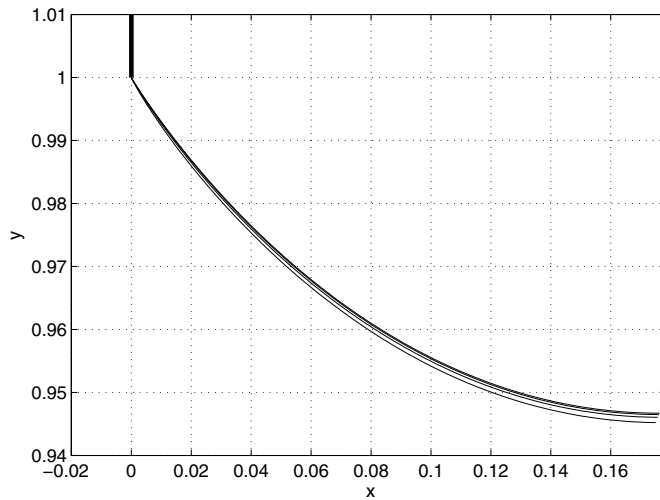
FIG. 6.4. *The free-streamline for the two-dimensional supersonic jet with $M_* = 2$ at the resolutions of Table 6.1(b). Coarse grid gives the lower line and the fine grid the upper line.*

to nonlinearity. It is easier to estimate the choke point M_{*c} simply by observing when the discharge coefficient first levels off, say to 3 decimal places.

• Along the sonic line, for the supersonic jet, it is possible to use either central differences of the subsonic region or backward differences. The results here have been obtained using central differences.

7. Conclusions. The hodograph transformation method is extended here to solve supercritical nozzle flows for any Mach number. The method does not require

matching along the sonic line as the entire problem is solved directly and simultaneously for both regions subsonic and supersonic. The hodograph plane is extended into a rectangular domain which is more convenient for applying the finite difference approximations than using a characteristic as a boundary. This allows for better applicability resulting in an efficient method and in improvements in execution time.

For fixed δ, the solution to the two-dimensional or axisymmetric nozzle problem is a one-parameter solution: the discharge coefficient depends on the pressure ratio. When the pressure ratio is close to unity, the gas velocity and compressibility effects are small. The critical pressure ratio is particularly important as it defines the transition from subsonic to supersonic flow. Solutions in this paper are obtained for gas expanding into near vacuum. Under vacuum conditions, (4.7) shows that flow around the corner B turns by a maximum angle $\theta_\infty = (\sqrt{b} - 1)\pi/2$, which is the maximum possible deflection in a Prandtl–Meyer expansion fan. Thus, the bounding streamline turns at B from $\theta = \delta$ to a limiting value $\theta = \theta_\infty + \delta$. Point D goes past line CU, but it is still possible to solve in a rectangular domain, as shown in Figure 7.1, where the whole region $BAUD'$ maps into the corner of the wall. The speed at D' is $M_* = 2.32755$. The hodograph domain also shows that the jet continues to expand as it travels away from the exit plane to the limiting angle θ_∞. This shows that gas turns far downstream to a flow direction angle beyond $-\delta$.
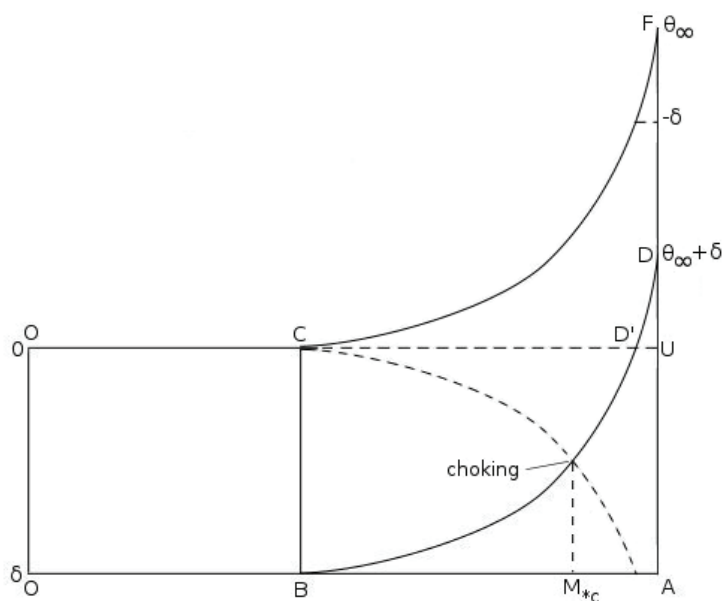

FIG. 7.1. *The hodograph domain corresponding to nozzle flow expanding into vacuum. A solution can be obtained in the rectangular region $OAUO$.*

Centered differences can also be applied in the supersonic region of the hodograph plane as an alternative to first order accurate backward differences. An advantage is that they are second order accurate; a disadvantage is that the scheme is then conditionally stable. Von Neumann stability analysis applied to the planar flow governing equation yields the stability condition

(7.1) $$\left(\frac{\Delta\theta}{\Delta M_*}\right)^2 \leq -\frac{f(M_*)}{M_*^2}.$$

Equation (2.15) shows that the Γ-characteristics meet the sonic line perpendicularly, and thus (7.1) leads to severe restrictions on the time-like step $\Delta\theta$ in the supersonic region near the sonic line for given ΔM_*. However, centered differences can be used away from this region in a mixed scheme consisting of backward and centered differences.

The hodograph technique presented here can also be applied to incompressible flows through gaps, as the shallow water equations are identical to the compressible flow equations if the depth of the fluid is replaced by the density and ratio of specific heats set to $\gamma = 2$ [11].

7.1. Jet instability. A very sharp nozzle lip and the assumption of frictionless, irrotational flow are idealizations. In practice there will be interaction between the medium and the fluid, and between the jet surface and downstream atmosphere. The irrotationality assumption will also be violated by shocks in the supersonic case, but these occur further downstream and do not concern the present study. The effects of viscosity and the effects of departure from the ideal requirements of a sharp lip at the nozzle exit are discussed in more detail by Alder [4].

The flows computed here are steady solutions of the nonlinear inviscid equations, and so it is important to consider the existence and nature of any instabilities to which they might be susceptible. Experimental studies of jets issuing from convergent-divergent nozzles have identified three families of instability waves; see Oertel [12, 13, 14]. Theoretical analyses [15, 16] show that high-speed jets with thin mixing layers support families of subsonic, supersonic, and Kelvin–Helmholtz instability waves. Tam and Hu [15] note that Kelvin–Helmholtz instability waves are key to the formation of large scale turbulence structures in jets and the associated turbulent mixing noise. Moreover, for imperfectly expanded jets, the quasi-periodic shock cell structure causes the radiation of additional noise: broadband shock-associated noise and screech tones. Tam [17] investigates the noise generation mechanism of these components of supersonic jet noise. The rapidly varying flow geometry here differs significantly from the majority of theoretical studies where the mean flow is independent of axial distance along the jet or slowly varying along the jet [16, section 6A] and so, since even small divergence affects flow instability characteristics [18], instabilities here can be expected to differ significantly from those of nondivergent jets. The slowly varying matched asymptotic expansion methods reviewed by Morris [16] are no longer applicable to the present geometry, but the present easily computed highly accurate steady solutions offer the possibility of direct numerical solution of the two-dimensional stability eigenvalue problem for a range of parameter values. This remains a sizable computational task and will not be discussed further here.

REFERENCES

[1] S. A. CHAPLYGIN, *Gas Jets*, NACA TM 1063, National Advisory Committee for Aeronautics, Washington, D.C., 1944.

[2] F. I. FRANKL, *The flow of a supersonic jet from a vessel with plane walls*, Dokl. Akad. Nauk SSSR, 58 (1947), pp. 381–384.

[3] R. E. NORWOOD, *Two-dimensional transonic gas jets*, in Proceedings of the 4th U.S. National Congress of Applied Mechanics, Vol. 2, 1962, pp. 1359–1367.

[4] G. M. ALDER, *Transonic Flow through Sharp-Lipped Convergent Nozzles*, Ph.D. thesis, University of Edinburgh, UK, 1976.

[5] L. P. COOK, E. NEWMAN, S. RIMBEY, AND G. SCHLEINIGER, *Sonic and subsonic axisymmetric nozzle flows*, SIAM J. Appl. Math., 59 (1999), pp. 1812–1824.

[6] R. COURANT AND K. O. FRIEDRICHS, *Supersonic Flow and Shock Waves*, Interscience Publishers, New York, 1948.

[7]   K. G. GUDERLEY, *The Theory of Transonic Flow*, Pergamon Press, Elmsford, NY, 1962.
[8]   C. J. CHAPMAN, *High Speed Flow*, Cambridge University Press, Cambridge, UK, 2000.
[9]   L. V. OVSIANNIKOV, *Gas flow with straight transition line*, Akad. Nank SSSR Prikl. Mat. Meh., 13 (1949), pp. 537–542.
[10] R. S. BENSON AND D. E. POOL, *Compressible flow through a two-dimensional slit*, Internat. J. Mech. Sci., 7 (1964), pp. 315–366.
[11] O. KRYEZIU, *Rotating and Non-rotating Flows through Gaps by the Hodograph Method*, Ph.D. thesis, University College London, 2011.
[12] H. OERTEL, *Mach wave radiation of hot supersonic jets*, in Mechanics of Sound Generation in Flows, E. A. Muller, ed., Springer-Verlag, New York, 1979, pp. 271–281.
[13] H. OERTEL, *Mach wave radiation of hot supersonic jets investigated by means of the shock tube and new optical techniques*, in Proceedings of the 10th International Symposium on Shock Tubes and Waves, A. Lifshitz and J. Rom, eds., Jerusalem, 1980, pp. 266–275.
[14] H. OERTEL, *Coherent structures producing Mach waves inside and outside of the supersonic jet*, in Structure of Complex Shear Flow, E. R. Dumas and L. Fulachier, eds., Springer-Verlag, New York, 1982, pp. 334–343.
[15] C. K. W. TAM AND F. Q. HU, *On the three families of instability waves of high-speed jets*, J. Fluid Mech., 201 (1989), pp. 447–483.
[16] P. J. MORRIS, *The instability of high speed jets*, Internat. J. Aeroacoust., 9(1–2) (2010), pp. 1–50.
[17] C. K. W. TAM, *Supersonic jet noise*, Annu. Rev. Fluid Mech., 27 (1995), pp. 17–43.
[18] C. K. W. TAM AND P. J. MORRIS, *The radiation of sound by the instability waves of a compressible plane turbulent shear layer*, J. Fluid Mech., 98 (1980), pp. 349–381.